Degenerate parabolic models for sand slides

Applied Mathematical Modelling 89 (2021) 1627–1639

Contents lists available at ScienceDirect

Applied Mathematical Modelling

journal homepage: www.elsevier.com/locate/apm

Degenerate parabolic models for sand slides

Roberto Nuca[a,b,c], Andrea Lo Giudice[c], Luigi Preziosi[a,*]

[a] Department of Mathematical Sciences "G. L. Lagrange", Dipartimento di Eccellenza 2018-2022, Politecnico di Torino, Corso Duca degli Abruzzi 24, Torino 10129, Italy
[b] Department of Mathematics "G. Peano", Via Carlo Alberto 10, Torino 10123, Italy
[c] Optiflow Company, 160 Chemin de la Madrague-Ville, Marseille 13015, France

ARTICLE INFO

Article history:
Received 11 March 2020
Revised 18 July 2020
Accepted 2 August 2020
Available online 13 August 2020

Keywords:
Degenerate parabolic equations
Non-Newtonian fluids
Sand
Sand avalanche
Granular materials
Non-linear diffusion

ABSTRACT

The morphodynamic evolution of the shape of dunes and piles of granular material is largely dictated by avalanching phenomena, acting when the local slope gets steeper than a critical repose angle. A class of degenerate parabolic models are proposed closing a mass balance equation with several viscoplastic constitutive laws to describe the motion of the sliding layer. Comparison among them is carried out by means of computational simulations putting in evidence the features that depend on the closure constitutive assumption and the robust aspects of the models. The versatility of the model is shown applying it to the movement of sand in presence of walls, open ends, columns, doors, and in complicated geometries.

1. Introduction

Four phenomena contribute to wind-induced sand movement and eventually to the formation and evolution of dunes: erosion from the sand bed, transport by the wind, sedimentation due to gravity, and sand grain slides occurring when the slope of the accumulated sand exceeds a critical repose angle [1] that depends on the specific granular material [2]. In particular, erosion, sedimentation, and sand sliding determine the evolution of the free-boundary over which wind blows and transports the sand. As explained in detail in [3] and in the recent review [4], the need of coupling a multiphase turbulent fluid-dynamics model with the morphodynamics of the sand surface requires the deduction of mathematical models for such phenomena that are able to describe the evolution of the sand bed in a way that is at the same time accurate and computationally fast. However, applications are not restricted to sand dynamics but can be extended to debris and other granular material in general as they present similar behaviours.

Referring again to [4] for a more detailed review, many modeling frameworks were developed to study the phenomena involved, both for sand and snow, and for other granular materials in general. Savage and Hutter [5] proposed a hydrodynamical models, based on Saint-Venant equations. They start from the incompressibility condition and momentum conservation equations in the flowing layer and then integrate them over the thickness of the rolling layer, not considering erosion and deposition. This gap was then filled, for instance, by Douady et al. [6], Khakhar et al. [7] and Gray [8]. A detailed analytical study of Savage and Hutter's model was performed by Colombo et al. [9].

* Corresponding author.
E-mail address: luigi.preziosi@polito.it (L. Preziosi).

https://doi.org/10.1016/j.apm.2020.08.018

Variational approaches have been proposed as well. Firstly, Aronsson et al. [10] introduced the p-Laplacian operator in order to model a non-homogeneous superficial diffusion to determine the height of a growing pile of a noncohesive sand. Mathematical properties were studied in a functional analysis framework by focusing on the theoretical results when the parameter p tends to infinity. Prigozhin [11] developed a variational model based on mass balance for the sand pile and assuming the surface flow is directed down in the direction of steepest descent subject to a slope constraint. Prigozhin et al. [12] allowed a leading coefficient to vanish if the slope is below a threshold corresponding to the repose angle.

Bouchaud and coworkers [13,14] divided the sand pile in a static zone and a moving layer, giving rise to the so-called *two-layers models*. Such models are characterized by two state variables, the local height of the static part and the local density (or height) of the rolling layer, linked by an exchange term which governs the transfer of mass from one status to the other. Of course, in the static zone the advection velocity vanishes, while in the rolling layer it is usually considered constant and strictly positive downhill. Also de Gennes and coauthors [15–18] and Prigozhin and Zaltzman [12] proposed modified versions of this type of models, with the latter that assumed a proportionality of the drift velocity with the gradient of the height of the sandpile. In the models proposed by Hadeler and Kuttler [19–21], velocity is again constant, though it is mentioned that it might depend on the slope (see, for instance, [22]). An exchange term proportional to the difference between the slope of the sand bed and the repose angle governs the transfer of sand between the static and the rolling layer.

A detailed analytical study of two-layers models was performed by Cannarsa and coworkers [23–26] for different boundary conditions. Falcone and Finzi Vita [27–29] instead focused on the proper numerical method to integrate two-layers models putting in evidence some unrealistic features such as the presence of blow-ups when the boundary of the domain changes type, e.g., from a wall to an open end. Others are (i) the formation of artificial valleys on the top of the sand pile obtained by pouring sand on its top, due to the discontinuity of downhill velocities on the two slopes in 1D simulations, or in situations in which the maximum height of the sand pile should be reached close to a wall; (ii) the dependence of the evolution and of the final configuration from the non-uniquely defined initial partitioning of the sand pile in a static and a rolling region, e.g., if all the mass is set to be initially static, then there is no evolution even if the initial configuration exceeds the repose angle.

Starting from the just mentioned computational needs [3,4], in [30] we proposed a model for the height of the sand pile that does not present the problems mentioned above. It is based on a reduction of a mass balance equation obtained assuming that (i) the thickness of the sliding layer is small, (ii) the grains move along the direction of steepest descent, (iii) the speed is given by the limit velocity of a body sliding down a slope under the action of gravity, Coulomb friction, and a drag force taken to be proportional to the sliding speed.

It is proved that assumptions (i) and (ii) lead to an evolution equation for the height $h(x, y, t)$ of the sand pile with the following structure

$$\frac{\partial h}{\partial t} = \nu \nabla \cdot \left[f_{sl}(|\nabla h|) \frac{\nabla h}{|\nabla h|} \right] + q, \tag{1}$$

where f_{sl} is called the sliding term, related to the mean sliding speed w through the relation $f_{sl}(|\nabla h|) = \frac{\delta}{\nu} w(|\nabla h|)$ where δ is the thickness of the sliding layer and ν is an effective diffusion coefficient. The last term q in (1) takes into account of external volume supplies of sand per unit area. The existence of a repose angle triggering the motion of the sand grains reflects into the fact that the sliding term vanishes for slopes, and therefore $|\nabla h|$, below a threhsold value. This gives to the parabolic equation (1) a degenerate character, that justifies calling this type of models Degenerate Parabolic Sliding Models (in the following shortened as DPSMs).

Specifically, in [30] assumption (iii) led to

$$f_{sl}(|\nabla h|) = \frac{(|\nabla h| - \tan \alpha_{cr})_+}{\sqrt{1 + |\nabla h|^2}}, \tag{2}$$

where $(g)_+ = (g + |g|)/2$ stands for the positive part of g, so that f_{sl} vanishes when $|\nabla h| \leq \tan \alpha_{cr}$, where α_{cr} is the repose angle.

Of course, it is possible to model in other ways the complex fluid-like behavior of the thin layer sliding on the top of the sand pile when the angle of steepest descent is larger than the repose angle (a configuration that will be called supercritical in the following), giving rise to different sliding terms f_{sl}. In particular, still working under the hypotheses (i) and (ii) above, we here consider several viscoplastic constitutive models named after Bingham, Casson, and Herschel-Bulkley (see, for instance [31,32] for more details). All these models are characterized by the presence of a yield stress that must be overcome before the material can flow. This common feature is related to the existence of a repose angle for the sand pile. Exploiting the fact that for these models it is possible to determine the velocity profile of a flow down an inclined plane, our aim is to extend DPSMs to different closures and to point out robust features and evolutionary differences among the mathematical models.

As we shall see, regardless of the constitutive closure, in spite of their simplicity, all the models above reply many well known features of sand slides, such as the non-uniqueness of static configurations in subcritical conditions, i.e., with slopes always smaller than the angle of repose and the link between critical stationary configurations and the solution of the same eikonal equation. So, starting from supercritical conditions the solution of all models tends towards an equilibrium identified by the same equation. The difference is in the way this solution is reached, especially when the slope gets close

to the repose angle, with the model (1)–(2) being the fastest to reach the equilibrium and the one in which the closure is achieved using a Herschel-Bulckley constitutive equations with a small power being the slowest.

The paper is organized as follows. In Section 2 we derive the viscoplastic closures of the DPSM, starting from different constitutive laws. Section 3 presents the result of comparative tests between the different models obtained, in order to evaluate the differences between them in terms of final configuration and convergence speed. Some examples of application of the models in practical situations are given in Section 4. A final discussion section concludes the paper.

2. Viscoplastic models for the sliding speed

Modelling the motion of granular materials can be rather complicated, especially when there is massive relative motion among the grains. Luckily, in many situations involving the redistribution of the granular mass, the motion is limited to a sliding layer that has a thickness much smaller than the characteristic dimension of the sand pile. This suggests to work with integrated variable on the thickness of the moving layer. Having this in mind, we will assume that the thickness of the sliding layer is small and constant δ and that the behaviour of the ensemble of sand grains is fluid-like with viscoplastic characteristics.

So, coming briefly to the deduction of the model and referring to [30] for more details, we consider a control volume $\mathcal{V}$ with vertical lateral surface and the basis $\mathcal{A}$ deep in the sand. The integral form of the mass balance equation then writes as

$$\frac{d}{dt}\int_{\mathcal{A}} \rho h \, dA = -\int_{\partial\mathcal{V}_{air}} \mathbf{q}\cdot\mathbf{n}\, d\Sigma - \int_{\partial\mathcal{V}\cap\mathcal{S}} \rho\mathbf{v}\cdot\mathbf{n}\, d\Sigma\,,$$

where ρ is the sand density and $h(x, y, t)$ is the height of the sand pile. The first integral on the rhs refers to the sand flux sedimenting through the top and the second one to that within the thin creep layer denoted by $\mathcal{S}$.

We then assume that sand grains slide along the surface $h(x, y, t)$ in the direction of the steepest gradient

$$\mathbf{t} = -\frac{\nabla h + |\nabla h|^2\mathbf{k}}{|\nabla h|\sqrt{1+|\nabla h|^2}}\,,$$

with speed w, that depends on the local slope of the surface, so that $\mathbf{v} = w\mathbf{t}$. Therefore, one can re-write the sand flux within the thin creep layer as

$$\int_{\partial\mathcal{V}\cap\mathcal{S}} \rho\mathbf{v}\cdot\mathbf{n}\, d\Sigma = \int_{\partial\mathcal{A}} \rho w\delta \frac{\mathbf{t}\cdot\mathbf{n}}{|\mathbf{t}\cdot\mathbf{n}|}\, d\Gamma = -\int_{\mathcal{A}} \nabla\cdot\left(\rho w\delta\frac{\nabla h}{|\nabla h|}\right) dA\,,$$

where we used the fact that we can rewrite the surface element as $d\Sigma = \frac{\delta}{\cos\theta} w(|\nabla h|) = \frac{\delta}{|\mathbf{t}\cdot\mathbf{n}|} c$ where $d\Gamma$ is the line element along ∂A and that the lateral walls are vertical.

Defining $q := -\mathbf{q}\cdot\mathbf{k}/\rho$ and $\nu f_{sl}(|\nabla h|) := w(|\nabla h|)\delta$ where ν is an effective diffusion coefficient and f_{sl} is a dimensionless term that we will call sliding term because of its dependence from $|\nabla h|$ we finally have

$$\frac{\partial h}{\partial t} = \nu\nabla\cdot\left[f_{sl}(|\nabla h|)\frac{\nabla h}{|\nabla h|}\right] + q. \tag{3}$$

The crucial point is now to evaluate the sliding speed w or equivalently f_{sl}. However, as we shall see the existence of a minimal slope triggering the motion of the grains implies that f_{sl} vanishes below a certain threshold for $|\nabla h|$ giving (3) a degenerate character. For sake of clarity, we explicitly remark that for this reason we extend to zero the value of the square parenthesis in (3) when $|\nabla h| = 0$.

In order to identify the mean sliding speed we work in the vertical plane containing the direction of steepest gradient $\mathbf{t}$ represented in Figure 1 and assume that in the thin sliding layer the velocity profile can be approximated to that of a viscoplastic fluid flowing down an inclined plane with slope α, such that $\tan\alpha = |\nabla h|$. In this geometry, neglecting inertia, the equilibrium of forces locally reads

$$\frac{\partial T_{x'y'}}{\partial y'} = -\rho g\sin\alpha\,,$$

where $T_{x'y'}$ is the shear stress and g is the gravitational acceleration. The above equation joined with stress-free boundary condition at the free surface

$$T_{x'y'}\Big|_{y'=\delta} = 0\,,$$

can be trivially integrated to give the shear stress

$$T_{x'y'} = \rho g(\delta - y')\sin\alpha. \tag{4}$$

If we take now constitutive models characterized by the presence of a yield stress τ, then there is flow only if an invariant measure of the stress is above it. One of the most common yielding criteria in viscoplastic flows is based on

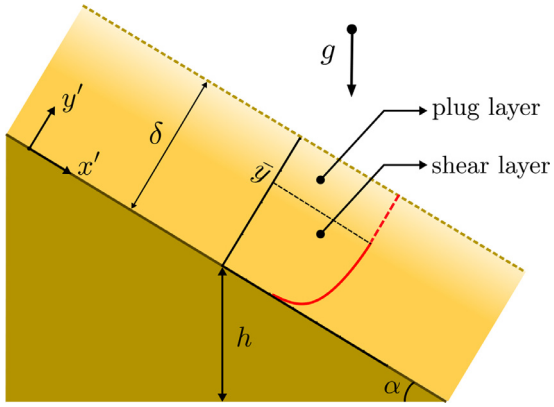

Fig. 1. Velocity profile within a layer of moving sand behaving like a viscoplastic fluid in the vertical section containing the direction of steepest descent. The layer has thickness δ and $\bar{y}$ distinguishes the shear layer for $y' < \bar{y}$ (full curve) from the plug layer for $y' > \bar{y}$ (dashed curve).

the second invariant of the stress tensor [31,32], that in the two-dimensional section of our interest writes $|T_{x'y'}| > \tau$: This means that there is flow only if

$$\sin\alpha > \sin\alpha_{cr} := \frac{\tau}{\rho g \delta},$$

so that α_{cr} represents the repose angle. We will call this case supercritical, while we will call subcritical a configuration with $\alpha < \alpha_{cr}$ everywhere. In this case, as shown in Fig. 1, the upper layer

$$y' > \bar{y} := \delta\left(1 - \frac{\sin\alpha_{cr}}{\sin\alpha}\right),$$

is a plug layer moving rigidly with the same velocity, while the lower layer $y' < \bar{y}$ where $T_{x'y'} > \tau$ undergoes a shear flow. We observe that at $y' = \bar{y}$ the shear stress is continuous and equal to τ.

At this point, in order to proceed further and explicit the velocity profile in the supercritical case $\alpha > \alpha_{cr}$, we need to specify the constitutive equation. In the following we will use, as examples, the widely used models by Bingham, Casson, and Herschel-Bulkley because they allow to determine the analytical expression of the velocity profile.

2.1. Herschel-Bulkley model

The Herschel-Bulkley constitutive model writes as

$$\mathbf{T} = \left[k\sqrt{|\mathrm{II}_{2\mathbf{D}}|^{\gamma-1}} + \frac{\tau}{\sqrt{|\mathrm{II}_{2\mathbf{D}}|}}\right] 2\mathbf{D}, \qquad \text{if} \quad \mathrm{II}_{\mathbf{T}} > \tau^2,$$

where $\mathbf{D} = \frac{1}{2}(\nabla\mathbf{v} + \nabla\mathbf{v}^T)$ is the rate of strain tensor, $\mathrm{II}_{2\mathbf{D}}$ is the second invariant of $2\mathbf{D}$ and $\mathrm{II}_{\mathbf{T}}$ the one of the stress tensor (see, for instance [31,32] for more details). If, instead, $\mathrm{II}_{\mathbf{T}} < \tau^2$, then the shear rate vanishes. In two-dimensions it reduces to

$$T_{x'y'} = \tau + k\left|\frac{\partial v_{x'}}{\partial y'}\right|^{\gamma}, \tag{5}$$

where $T_{x'y'} > \tau$ and $v_{x'}$ constant elsewhere. Then, in the shear layer $y' < \bar{y}$ Eq. (4) rewrites as

$$\frac{\partial v_{x'}}{\partial y'} = \left(\frac{\tau}{k}\right)^{1/\gamma}\left[\frac{\sin\alpha}{\sin\alpha_{cr}}\left(1 - \frac{y'}{\delta}\right) - 1\right]^{\frac{1}{\gamma}}, \tag{6}$$

that need be solved with the no-slip boundary condition at $y' = 0$. Because of the action of gravity, the flow will be downhill for small y'. So, there $\frac{\partial v_{x'}}{\partial y'} > 0$ and, actually, the positive sign will be kept because of the stress-free boundary condition. Therefore, overall the velocity profile is given by

$$v_{x'}(y') = \begin{cases} \frac{A}{\beta}\left[(\beta-1)^{1+\frac{1}{\gamma}} - \left(\beta - 1 - \beta\frac{y'}{\delta}\right)^{1+\frac{1}{\gamma}}\right] & \text{if } y' < \bar{y}; \\ \frac{A}{\beta}(\beta-1)^{1+\frac{1}{\gamma}} & \text{if } y' \geq \bar{y}. \end{cases} \tag{7}$$

where

$$A = \left(\frac{\tau}{k}\right)^{\frac{1}{\gamma}} \delta \frac{\gamma}{\gamma+1}, \qquad \beta = \frac{\sin\alpha}{\sin\alpha_{cr}},$$

with $\beta > 1$ when and where $\alpha > \alpha_{cr}$. In deducing (7) we also used the continuity of the shear stress in $y' = \bar{y}$, that implies that $\partial v_{x'}/\partial y'$ vanishes, in addition, of course, to the continuity of $v_{x'}$.

The mean speed across the moving layer $y' \in [0, \delta]$

$$w = \frac{1}{\delta}\left\{\int_0^{\bar{y}} \frac{A}{\beta}\left[(\beta-1)^{1+\frac{1}{\gamma}} - \left(\beta - 1 - \beta\frac{y'}{\delta}\right)^{1+\frac{1}{\gamma}}\right] dy' + \int_{\bar{y}}^{\delta} \frac{A}{\beta}(\beta-1)^{1+\frac{1}{\gamma}} dy'\right\},$$

can then be used to close (3). In fact, one can specify

$$\nu = \left(\frac{\tau}{k}\right)^{1/\gamma} \frac{\gamma}{(1+\gamma)(1+2\gamma)}\delta^2, \tag{8}$$

and f_{sl} as the product of two factors: a regular term f_{reg} and a degenerate term f_{deg}

$$f_{sl}(|\nabla h|) = f_{reg}(|\nabla h|) f_{deg}(|\nabla h|), \tag{9}$$

that, recalling that $\sin\alpha$ is a function of the slope $h(\mathbf{x}, t)$ given by

$$\sin\alpha = \frac{|\nabla h|}{\sqrt{1+|\nabla h|^2}},$$

write as

$$f_{reg}(|\nabla h|) = \frac{\sin\alpha_{cr}}{\sin\alpha}\left(1 + \gamma + \gamma\frac{\sin\alpha_{cr}}{\sin\alpha}\right), \tag{10}$$

which is always positive, while

$$f_{deg}(|\nabla h|) = \left[\left(\frac{\sin\alpha}{\sin\alpha_{cr}} - 1\right)_+\right]^{1+\frac{1}{\gamma}}, \tag{11}$$

vanishes when $\alpha \le \alpha_{cr}$, i.e., when $|\nabla h| \le \tan\alpha_{cr}$. In fact, if $\alpha < \alpha_{cr}$, $T_{x'y'} < \tau$ and there is no flow. The presence of this last term is the one that gives the parabolic equation (1) its degenerate character.

2.2. Bingham model

As well known, Bingham constitutive model is a particular case of a Herschel-Bulkley model with $\gamma = 1$ (and k replaced by μ) [31,32]. Hence, from (8,10,11) we readily have

$$\nu = \frac{\tau\delta^2}{6\mu}, \tag{12}$$

$$f_{reg}(|\nabla h|) = \frac{\sin\alpha_{cr}}{\sin\alpha}\left(2 + \frac{\sin\alpha_{cr}}{\sin\alpha}\right), \tag{13}$$

and

$$f_{deg}(|\nabla h|) = \left[\left(\frac{\sin\alpha}{\sin\alpha_{cr}} - 1\right)_+\right]^2. \tag{14}$$

In particular, for the discussion to follow it is useful to observe that the degeneracy is quadratic, while for a Herschel-Bulkley model it goes like $1 + \frac{1}{\gamma}$.

2.3. Casson model

Casson's constitutive model can be written in three dimensions as

$$\mathbf{T} = \left[\sqrt{\mu} + \frac{\sqrt{\tau}}{|\mathbb{I}_{2\mathbf{D}}|^{1/4}}\right]^2 2\mathbf{D}, \qquad \text{if} \quad \mathbb{I}_{\mathbf{T}} > \tau^2.$$

(see, for instance, [31,32] for more details) that in the two-dimensional section of our interest reduces to

$$\sqrt{T_{x'y'}} = \sqrt{\tau} + \sqrt{\mu\left|\frac{\partial v_{x'}}{\partial y'}\right|}. \tag{15}$$

Proceeding as in Section 2.1, one has then to solve the differential equation

$$\frac{\partial v_{x'}}{\partial y'} = \frac{1}{\mu}\left(\sqrt{\rho g(\delta - y')\sin\alpha} - \sqrt{\tau}\right)^2 = \frac{\tau}{\mu}\left(\sqrt{\beta}\sqrt{1-\frac{y'}{\delta}} - 1\right)^2,$$

with no-slip boundary condition at $y' = 0$. The velocity profile is then

$$v_{x'}(y') = \begin{cases} \frac{\tau\delta^2}{6\mu\beta}\left[\left(\sqrt{\beta}-1\right)^3\left(3\sqrt{\beta}+1\right) - \left(\sqrt{\beta}\sqrt{1-\frac{y'}{\delta}}-1\right)^3\left(3\sqrt{\beta}\sqrt{1-\frac{y'}{\delta}}+1\right)\right] & \text{if } y' < \bar{y}; \\ \frac{\tau\delta^2}{6\mu\beta}\left(\sqrt{\beta}-1\right)^3\left(3\sqrt{\beta}+1\right) \qquad \text{if } y' \geq \bar{y}. \end{cases} \tag{16}$$

The mean speed across the moving layer $y' \in [0, \delta]$ can again be written as $w = \frac{\nu}{\delta} f_{reg}(|\nabla h|) f_{deg}(|\nabla h|)$ with $\nu = \frac{\tau\delta^2}{30\mu}$,

$$f_{reg}(|\nabla h|) = \frac{\sin^2\alpha_{cr}}{\sin^2\alpha}\left(10\frac{\sin^{3/2}\alpha}{\sin^{3/2}\alpha_{cr}} + 6\frac{\sin\alpha}{\sin\alpha_{cr}} + 3\frac{\sin^{1/2}\alpha}{\sin^{1/2}\alpha_{cr}} + 1\right), \tag{17}$$

and

$$f_{deg}(|\nabla h|) = \left[\left(\sqrt{\frac{\sin\alpha}{\sin\alpha_{cr}}} - 1\right)_+\right]^3, \tag{18}$$

where we also considered the fact that if $\alpha < \alpha_{cr}$, $T_{x'y'} < \tau$ and there is no flow.

3. Comparison of slope evolutions

From the structure of the equation it is clear that in absence of any mass input q, every subcritical configuration with $h(\mathbf{x})$ such that $|\nabla h| \leq \tan\alpha_{cr}$, $\forall \mathbf{x}$ is a stationary solution, because f_{deg} in (11), (14), (18), as well as in (2), always vanishes being the angle of steepest descent $\alpha < \alpha_{cr}$.

On the other hand, starting from an initial condition such that $|\nabla h| > \tan\alpha_{cr}$ everywhere, then the evolution will tend to a solution of $f_{deg}(|\nabla h|) = 0$. Now, regardless of the closure assumption used, and therefore of the sliding model, this configuration is a solution of the eikonal equation $|\nabla h| = \tan\alpha_{cr}$, which then represents a robust feature of all the DPSMs proposed here and in [30].

Therefore, in order to put in evidence the differences among the models proposed above one should not look at the stationary configurations, but at transient behaviors. In order to do that, we will then integrate

$$\frac{\partial h}{\partial t} = \nu\nabla\cdot\left[f_{reg}(|\nabla h|) f_{deg}(|\nabla h|)\frac{\nabla h}{|\nabla h|}\right] + q, \tag{19}$$

with $f_{reg}(|\nabla h|) = 1/\sqrt{1+|\nabla h|^2}$ and $f_{deg}(|\nabla h|) = (|\nabla h| - \tan\alpha_{cr})_+$ in what we will call the Coulomb case, (10) and (11) in the Herschel-Bulkley case, (13) and (14) in the Bingham case, and (17) and (18) in the Casson case.

The main difference in the evolutions is due to the convexity of the curves representing the dependence of f_{sl} and specifically of f_{deg} on α close to α_{cr}. In fact, while the sliding term related to Coulomb's model goes linearly to zero, the other models have a stationary point there. More precisely, they behave like $(\alpha - \alpha_{cr})^n$ with $n = 2$ for Bingham model, $n = 1 + \frac{1}{\gamma}$ for Herschel-Bulkley models, and $n = 3$ for Casson model. This means that when approaching the repose angle the evolution becomes slower and slower especially for Casson fluids and Herschel-Bulkley models with $\gamma < 1$. The smaller γ is, the slower the process of approaching the stationary configuration is.

In Fig. 2 we plot the sliding velocity normalized with their maximum value obtained for $\alpha = 50^\circ$. From the figure it can be observed that at any angle the response to a Casson closure and to a Herschel-Bulkley one with $\gamma = 0.5$ are very close. So, we expect the evolutions related to them to be quite close.

Actually, it is useful to work in dimensionless variables scaling lengths with the reference size H of the sand pile, e.g., its height, and times with $T = \frac{H^2}{\nu f_{sl}(\alpha_*)}$ where α_* is a reference slope angle, so that

$$\frac{\partial \hat{h}}{\partial \hat{t}} = \hat{\nabla}\cdot\left[\frac{f_{reg}(\alpha) f_{deg}(\alpha)}{f_{reg}(\alpha_*) f_{deg}(\alpha_*)}\frac{\hat{\nabla}\hat{h}}{|\hat{\nabla}\hat{h}|}\right] + \hat{q},$$

the hats denote dimensionless variables.

In order to provide both a qualitative and quantitative comparison, DPMSs were implemented in the finite volumes open source code OpenFoam. Finite-volume methods were successfully used for degenerate parabolic problems (see for instance [33–35]). As concerns spatial discretion, the diffusive term is evaluated by means of Gauss theorem and mean value theorem. A generic diffusive term $\nabla\cdot(f_{sl}\nabla h)$ is written by means of normal boundary fluxes [36]

$$\nabla\cdot(f_{sl}\nabla h) = \frac{1}{V}\int_V \nabla\cdot(f_{sl}\nabla h)\,dV = \frac{1}{V}\oint_{\partial V} f_{sl}\nabla h\cdot d\mathbf{S} = \frac{1}{V}\sum_i^{nFaces} f_{sl}^f(\nabla h)_i^f\cdot\mathbf{S}_i^f,$$

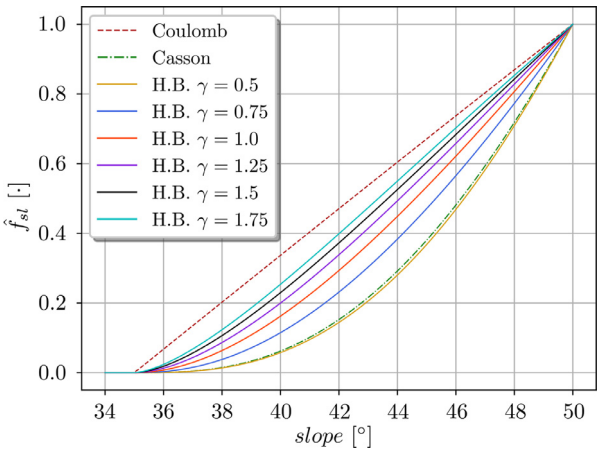

Fig. 2. Sliding term $\hat{f}_{sl}$ normalized with respect to the value achieved for a slope of 50° and a repose angle of $\alpha_{cr} = 35°$ for different DPSM closure assumptions. We recall that Bingham fluids correspond to a Herschel-Bulkley model with $\gamma = 1$.

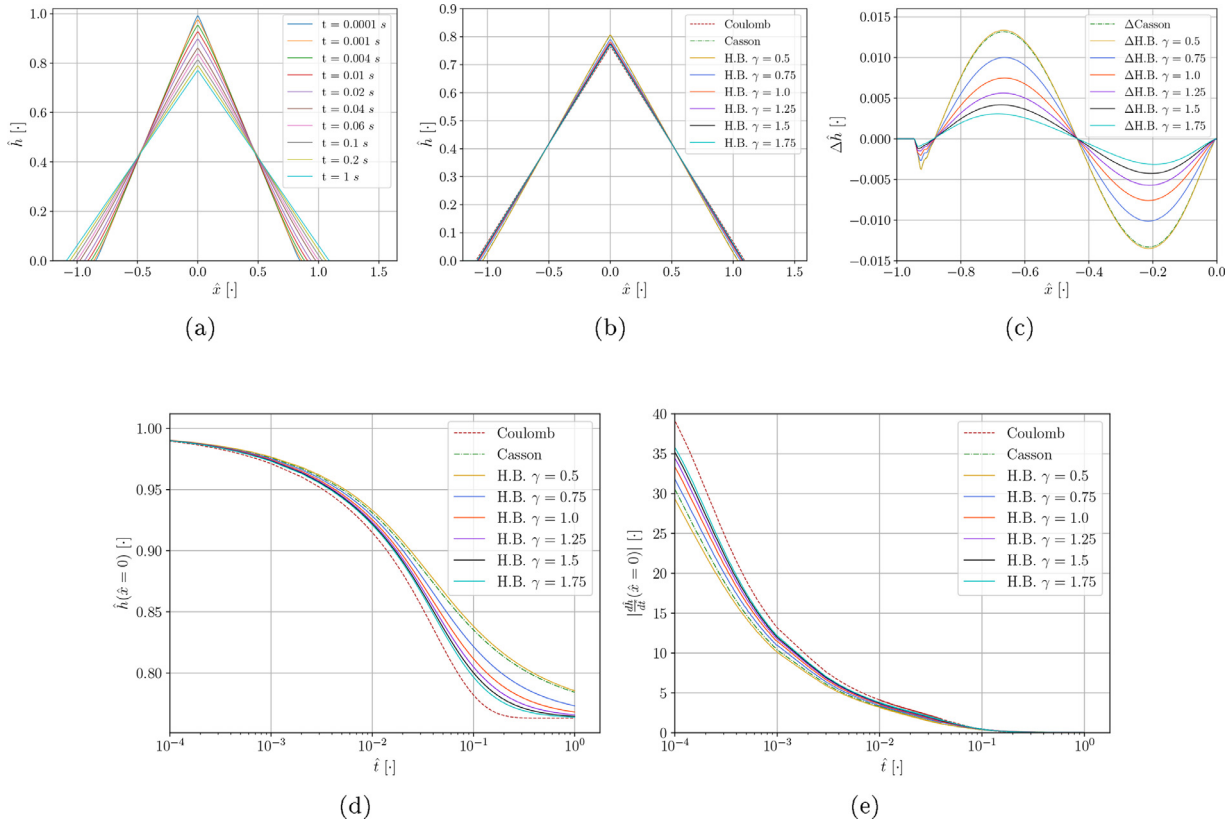

Fig. 3. (a) Spatial evolution of the profile of an initially supercritical conical sand pile with repose angle $\alpha_{cr} = 35°$ at different times for a Bingham closure. (b) Comparison of the configurations achieved using the different DPSMs at $\hat{t} = 0.5$. (c) Differences between the heights of the left slopes as obtained using the different viscoplastic models with that obtained using Coulomb closure at the time for which the configurations have maximum height equal to 0.8. Temporal evolution of the height $\hat{h}$ (d) and of the velocity of the tip of the sand pile (e) for the different models. Bingham model corresponds to $\gamma = 1$.

where f_{sl}^{f} is the face-interpolated value of the sliding term and $\mathbf{S}^{f}$ is the face area normal vector. Cubic interpolation is used to get cell-face values from cell-center ones. Consequently, where the diffusivity becomes zero, the parabolic equation degenerates to $\frac{\partial h}{\partial t} = q$ which can be simply integrated in time. An implicit Euler scheme is used for time discretization.

In order to show the effect of the different constitutive closures, we simulate the motion of a sand pile with an initially conic shape with an angle of $\alpha_{*} = 50°$ while the repose angle is 35°.

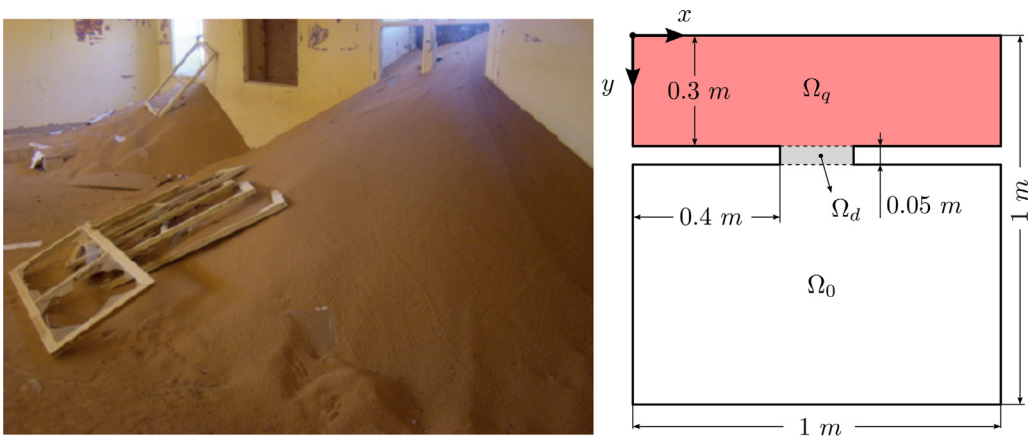

Fig. 4. Sand pile entering a room through an opening: (a) Real situation ([37], permission requested), (b) Sketch of the domain of integration close to one of the openings seen from the top.

In Fig. 3a the evolution is shown in the case in which the sliding layer is described as a Bingham fluid. The slope gradually decreases keeping an almost conical shape to eventually achieve the stationary configuration with an angle at the basis equal to the repose angle. In fact, as already stated, regardless of the closure assumption, all DPSMs relax an initial configuration that is supercritical everywhere, to the solution of the same eikonal equation, which in this case is a cone. In Fig. 3b we plot the configurations achieved using the different closures at $\hat{t} = 0.5$

In order to put in evidence how much the solutions differ and where, in Fig. 3c we plot the difference between the solution obtained by the viscoplastic models considered here with respect to the one obtained using Coulomb closure as a reference. The maximum difference is about 1.5% of the pile height.

The biggest discrepancy among the evolutions stays in how fast the tip of the cone moves down and the basis of the cone enlarges. In fact, as shown in Fig. 3d that plots the temporal evolution of the height of the sand pile, when the angle gets closer to the repose angle the asymptotic trend toward equilibrium differs more. In fact, the deceleration achieved using the different models deviate from each other because of the convexity properties mentioned above (see also Fig. 2). A difference evidentiated in Fig. 3d is the location of the inflection points of the curves in the semilog graph and consequently the logarithm of the durations of the phases where the curve is convex and concave. As a consequence, as shown in Fig. 3e the solution of the model with a Coulomb closure is the fastest and the one using a Casson fluid is the slowest (actually, the one using a Herschel-Bulkley fluid with $\gamma = 0.5$ is very close to it and if $\gamma < 0.5$ the asymptotic trend would be even slower).

The above discussion suggests that in order to identify the best closure, it is more useful to look at the temporal evolution of the sand pile tip or toe (e.g., Fig. 3d) and in particular to their speed as in Fig. 3e, rather than focusing on the spatial evolution of the slopes because they are very similar as shown in Fig. 3a,b. In this respect, Casson or Herschel-Bulkley closures with $\gamma < 1$ take much longer to reach asymptotically the stationary configuration with respect to Coulomb or Bingham closures and in this case even when the slope has an angle that is close to the repose angle, the solution still slowly moves so that it takes a long time to reach what can be considered a stop. On this basis we can state that Coulomb, Bingham or Herschel-Bulkley models with $\gamma > 1$ are more realistic than Casson or Herschel-Bulkley models with $\gamma < 1$.

On the other hand, if the main interest is in using a reliable model to get to the proper quasi-static configuration in a numerically efficient way, then Coulomb-like closure is certainly the best because it is the fastest to reach it without loosing accuracy.

4. Simulation in realistic set-ups

In this section we apply the model to more realistic set-ups, containing obstacles, walls and openings, also in presence of external sources. The first simulation regards the formation of a three-dimensional sand pile obtained constantly pouring sand in a region Ω_q on one side of a thick vertical wall (the shaded area in Fig. 4b). The wall presents a 0.2 m wide and 0.05 m thick central opening Ω_d leading to a region Ω_0 having all other sides open, in the sense that when sand reaches these boundaries it can freely flow down. From the mathematical point of view, this corresponds to Dirichlet boundary conditions, while no-flux boundary conditions need be applied on the walls. The set-up can mimick situations like those shown in Fig. 4a where sand came from outside the room and entered it through the openings in the walls.

Before starting the discussion, we observe that, as shown by Falcone and Finzi Vita [27–29] the change of boundary conditions may be troublesome leading to numerical problems and unphysical results more related to the mathematical model than to its numerical implementation. This is for instance the case of two-layer models. At variance with that, the

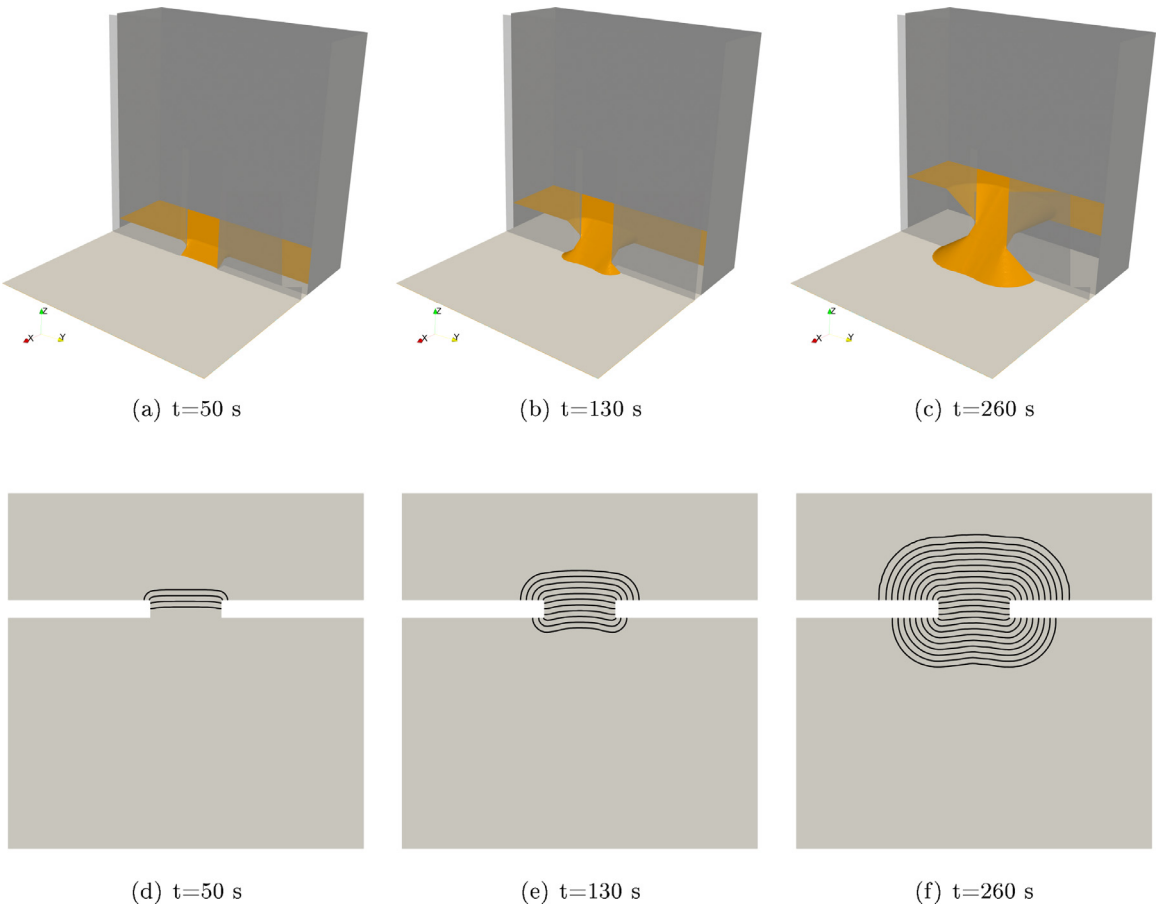

Fig. 5. Profiles of sand poured in the space beyond the door and exiting from it at early times. The sliding is achieved using the DPSM with a Coulomb closure. The bottom row reports the contor plots of the 3D configurations plotted in the top row.

DPSMs proposed here have no problem in dealing with changes in the boundary conditions and result very reliable in managing complex realistic situations and geometries.

In the simulation shown in Fig. 5 we modelled sand using a Coulomb-like closure with $\alpha_{cr} = 35^\circ$, $\nu = 0.1\,\frac{\mathrm{m}^2}{\mathrm{s}}$, and $q = 10^{-3}\,\frac{\mathrm{m}}{\mathrm{s}}$ in Ω_q, but the results are very similar for all the other constitutive equations.

Coming to the description of the evolution, at the very beginning the profile is flat between the walls in Ω_q, while close to the door sand flows down so that the sand profile takes a slope equal to the critical angle (see Fig. 5a). The contour line where the surface is no longer constant is parallel to the wall in correspondence of the door and forms two circular arcs in correspondence of its jambs (see Fig. 5d). After the sand slope with this triagular section has reached the other end of the wall, i.e. the boundary between Ω_d and Ω_0, the sand tends to spread also laterally to the right and to the left of the door. Closer to the jambs the shape is still conical (see Fig. 5b,e). The foot of the sand pile advances faster on the right and on the left because more sand arrives there turning around the jambs. In the section corresponding to the middle of the door the slope is flat and the sand pile takes the shape of an inclined plane (see Fig. 5c,f). Hence, the shape is prism-like closer to the center of the door and conic-like to its side. The steepest angle is always very close to the repose angle. Also within Ω_q the region in which the slope is non constant enlarges. Initially (see Fig. 5c,f) it has more or less a prism-like shape corresponding to the door and a conic-like one to its side. Then at about $t = 400$ s the slope change in correspondence of the door hits the top boundary of Ω_q opposite to the door (see Fig. 6a,d). After that, in Ω_q the sand profile takes a more funnel-like shape (see Fig. 6b,c), while in Ω_0 the conic shape enlarges till just before $t = 650$ s the basis of the conic-like shape reaches the open end boundary. At this point also along the wall the conical shape becomes flat with an inclination close to the repose angle. Eventually, the stationary configuration is reached because the mass influx in Ω_q balances the mass outflux through $\partial\Omega_0$.

We remark that the entire simulation is very realistic (see Supplementary Video 1) and can be obtained with low computational cost, so that the update of the sand free surface does not represents a bottleneck for the entire multiphase fluid dynamics simulation that need be performed to describe sand transport in environmental problems.

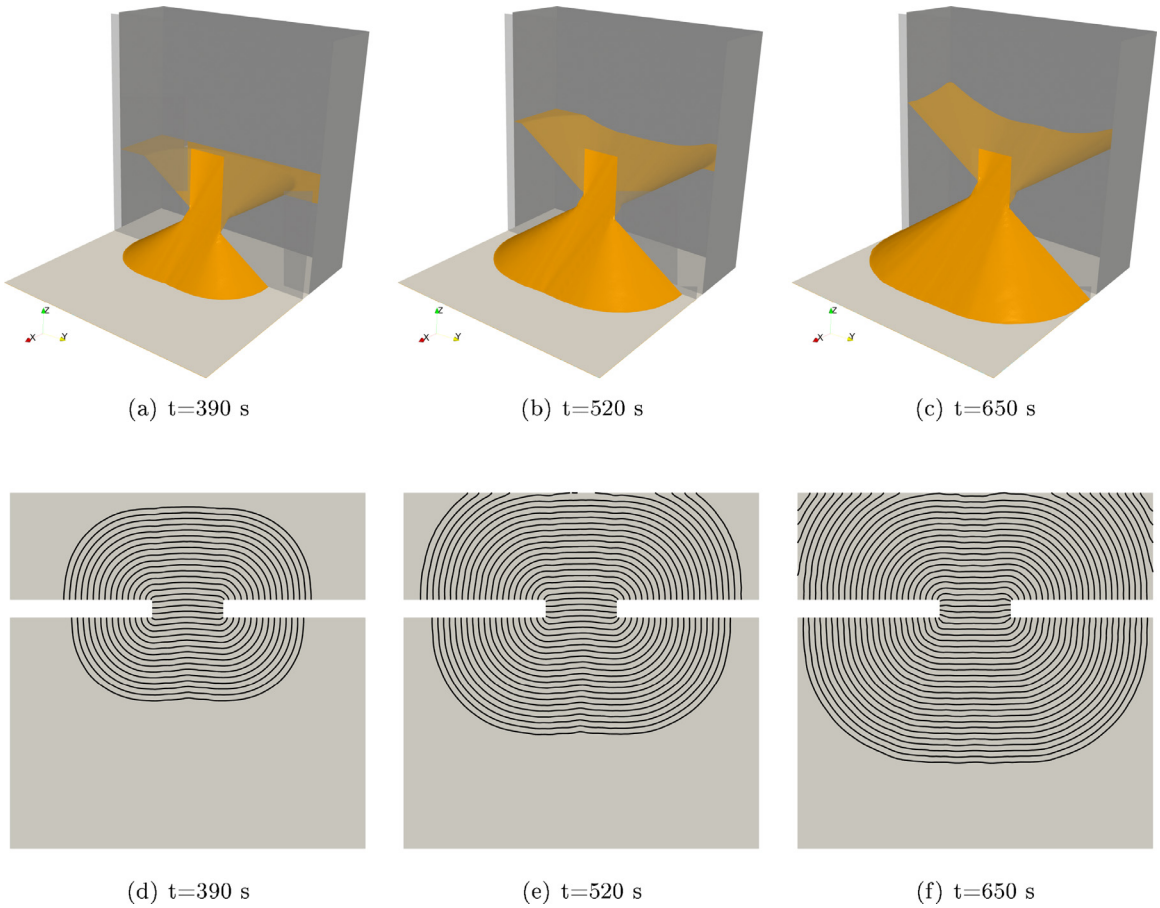

Fig. 6. Profiles of sand poured in the space beyond the door and exiting from it at later times. The profile shown in (f) is almost stationary. All the sand poured between the walls falls off the open boundaries to the right and to the left. The sliding is achieved using the DPSM with a Coulomb closure. The bottom row reports the contor plots of the 3D configurations plotted in the top row.

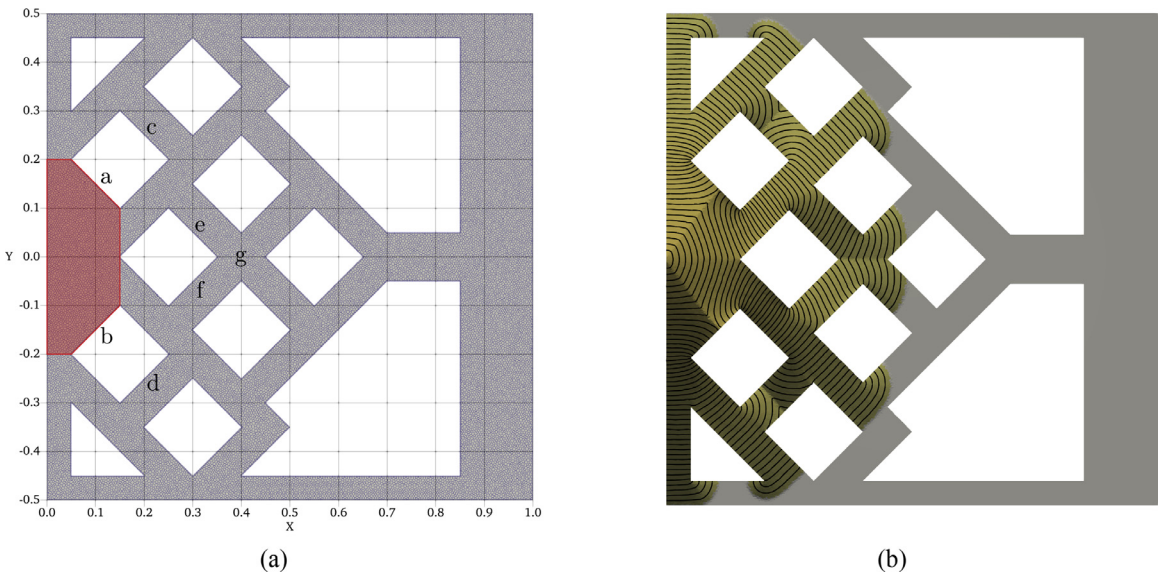

Fig. 7. (a) Domain of integration and numerical grid. The sand is poured in the shaded region in the grid. (b) Contour plot of the solution of the DPSM with Coulomb closure at $t = 840$ s. Corners in the contour plots correspond to slope discontinuities of the sand profile.

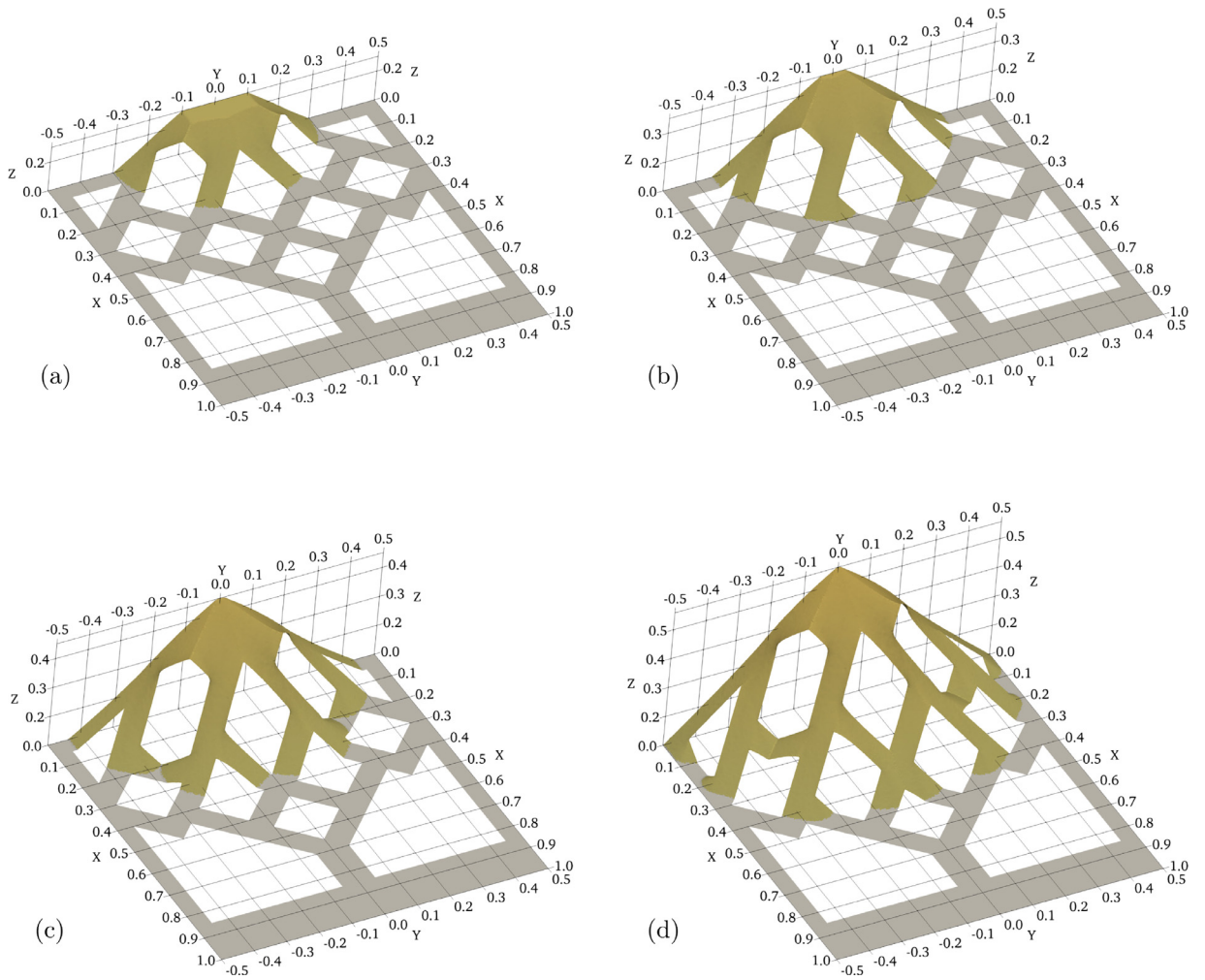

Fig. 8. Configurations of the sand pile poured in the region highlighted in Fig. 7a at different times $t = 150, 250, 450, 840$ s, respectively (a), (b), (c) and (d).

We notice, again, that the same final configuration is achieved with the viscoplastic closures and with Coulomb friction closure. Negligible differences in the evolution are present according to the constitutive closure used. Actually, as the flow is quasi-stationary, practically the configurations are a series of solutions of the eikonal equation. Differences increase with the increase of the flow rate q. However, we advise that the model might loose its validity for extremely high flow rates that may generate slopes that are much higher than the repose angle being closer to vertical slopes. In fact, in this case the hypothesis of small thickness of the sliding layer no longer holds. In spite of this, we mention that in [30] the model with a Coulomb-like closure was used to simulate experiments focusing on the collapse of initially cylindrical piles of sand, that of course start with a vertical wall, showing a satisfactory agreement.

As evident in Figs. 5–8, due to the degeneracy present in the model, a characteristic of the proposed DPSMs is the compact support of the solution starting from no sand and source term in a well defined area (and, of course, in other cases) and by the presence of slope discontinuities in the solutions. A basic example is the angle formed by the flat plane and the pile of sand or the angle between the horizontal profile in Ω_q and the sliding slope of the sand pile in Figs. 5 and 6. This is a characteristic of the solution of the eikonal equation as well.

A similar thing occurs when two sand piles encounter. In order to show how the model can easily reproduce such effects and handle complicate geometries, in Fig. 7–8 we focus on the interaction of sand with several columns and corridors placed in the room with three open ends and a wall at $x = 0$. Sand is continuously poured close to the wall for $x \leq 0.15$ m and $|y| \leq 0.2$ m at a rate of 2 mm/s, that is, the shaded area in Fig. 7a.

Starting from an empty configuration, the sand continuously supplied starts accumulating in the pentagonal area sliding on its sides passing from a sort of truncated pyramidal shape (notice the flat rectangle on the top of the sand pile in Fig. 8) to a full pyramidal-like shape with ridges, for instance, perpendicular to the sides of the columns denoted as **a** and **b** in Fig. 7a. In fact, the sand slides along the walls **a** and **b** from their centers in opposite directions turning around the corners

with a dynamics similar to the one in Fig. 5b,e. The ridge is also put in evidence in Fig. 7b by the presence of corners in the contour plots.

The sliding fronts then moves on the sides of the columns and then re-encounter on the other side of it forming a slope discontinuity. In fact, continuing to turn around the column, Fig. 8 presents the configuration after the sand piles coming from the left and the right of the same corridor **c** (and symmetrically **d**) encounter forming an angle $\pi - 2\alpha_{cr}$. After that the distribution of sand in the corridor preserves the angles close to the repose value α_{cr} but the level rises up because of the continuously incoming mass flux (see also Supplementary Video 2). A similar dynamics occurs in the crossing identified by **g** in Fig. 7a when the sand coming from the corridors **e** and **f** meets (see Fig. 8). Again such slope discontinuities correspond to corners in the contour plots in Fig. 7b.

As stressed several times along the paper, the evolution is very similar for all the closures considered above. For this reason, in Fig. 7–8 only the result for Coulomb closure is shown.

5. Conclusions and perspectives

In this work we have presented different closures of degenerate parabolic sliding models (DPSMs) to describe the morphology and evolution of sand piles studying similarities and differences. It is shown that DPSMs are reliable for many realistic situations characterized by negligible inertial effects and without massive motions of the granular material. The choice of the closure model is not crucial for the final configuration but affects the temporal evolution and the numerical convergence speed.

So, if the main interest is to describe in a precise way the evolution of the quasi-static shape of sand piles, it is not important which constitutive equation is chosen. In this respect, on the basis of our results, we can state that among them Coulomb-like closure is the most convenient one from the computational point of view, because it is the fastest to reach the stationary or quasi-stationary configuration without loosing accuracy.

If, instead the interest is in pointing out the difference among the different constitutive equations, these can be highlighted, for instance, focusing on the velocity and deceleration trends before reaching the stationary configuration and on the evolution of the compact support, if initial conditions and possibly source terms are giving rise to such solutions.

This gives rise to some interesting inverse problem questions related to how to identify in an efficient way the sliding term from experiments. To our knowledge inverse problems for nonlinear parabolic equations characterized by degeneracies driven by the gradient of the state variable have not been studied. Most works focus on the identification of the source term in the linear [38] and semilinear case [39–43] with the diffusion term only depending on space. Still working in this framework, Fragnelli et al. [44] instead focused on the identification of the space-dependent diffusion term. Much less is done when the diffusion term depends on the state variable. In some respect, the classical sedimentation model studied in [45] presents some similarities with DPSMs, because the diffusion term vanishes below a threshold value, but of the state variable, representing the volume ratio at which sedimenting particles start packing, rather then its gradient. In this case the numerical identification is obtained minimizing the L^2 norm of the volume ratio. The minimization of a suitable cost function is used in [46] where the diffusion coefficient depends on the gradient of the state variable as in DPSMs, but the parabolic equation is not degenerate. According to the discussion above, our impression that for DPSMs cost functionals based on the evolution of the boundary of the compact support and probably its velocity could be promising to better identify the form of the sliding term through the evaluation of its power law behavior for values of the slope close to the repose angle.

We recall that the applicability of the model becomes questionable when slopes are too strong and might trigger massive motion of sand, so that the smallness hypothesis on the thickness of the sliding layer and on the inertial effects that are fundamental to deduce the model can not be assured. In such cases more complicated models need be applied at the expenses of computational costs. However, an hypothesis that can be dropped is the constancy of the sliding layer, allowing it to be space dependent, though still small compared to the size of the sand pile.

Acknowledgment

Study developed in the framework of the Windblown Sand Modeling and Mitigation joint research, development and consulting group established between Politecnico di Torino and Optiflow Company and partially funded by INDAM, Regione Piemonte, and the MSCA-ITN-2016-EID SMaRT research project funded by the EU's Horizon 2020 research and innovation program under grant agreement No 721798.

Supplementary material

Supplementary material associated with this article can be found, in the online version, at doi:10.1016/j.apm.2020.08.018.

References

[1] M. Bretz, J. Cunningham, P. Kurczynski, F. Nori, Imaging of avalanches in granular materials, Phys. Rev. Lett. 69 (1992) 2431.
[2] T. Börzsönyi, T. Halsey, R. Ecke, Avalanche dynamics on a rough inclined plane, Phys. Rev. E 78 (1) (2008) 011306.

[3] A. Lo Giudice, L. Preziosi, A fully eulerian multiphase model of windblown sand coupled with morphodynamic evolution: erosion, transport, deposition, and avalanching, Appl. Math. Model. 79 (2020) 68–84.
[4] A. Lo Giudice, R. Nuca, L. Preziosi, N. Coste, Wind-blown particulate transport: a review of computational fluid dynamics models, Math. Eng. 1 (3) (2019) 508–547.
[5] S. Savage, K. Hutter, The motion of a finite mass of granular material down a rough incline, J. Fluid Mech. 199 (1989) 177–215.
[6] S. Douady, B. Andreotti, A. Daerr, On granular surface flow equations, Eur. Phys. J. B 11 (1999) 131–142.
[7] D. Khakhar, A. Orpe, P. Andresén, J. Ottino, Surface flow of granular materials: Model and experiments in heap formation, J. Fluid Mech. 441 (2001) 255–264.
[8] J. Gray, Granular flow in partially filled slowly rotating drums, J. Fluid Mech. 441 (2001) 1–29.
[9] R. Colombo, G. Guerra, F. Monti, Modelling the dynamics of granular matter, IMA J. Appl. Math. 77 (2) (2012) 140–156.
[10] G. Aronsson, L. Evans, Y. Wu, Fast-slow diffusion and growing sandpiles, SIAM J. Appl. Math. 131 (1996) 304–335.
[11] L. Prigozhin, Variational model of sandpile growth, Eur. J. Appl. Math. 7 (3) (1996) 225–235.
[12] L. Prigozhin, B. Zaltzman, Two continuous models for the dynamics of sandpile surfaces, Phys. Rev. E 63 (2001) 041505.
[13] J. Bouchaud, M. Cates, J. Prakash, A model for the dynamics of sandpile surfaces, J. Phys. I 4 (1994) 1383–1410.
[14] J. Bouchaud, M. Cates, J. Prakash, S. Edwards, Hysteresis and metastability in a continuum sandpile model, Phys. Rev. Lett. 74 (11) (1995) 1982–1985.
[15] P. de Gennes, Dynamique superficielle d'un matériau granulaire, C. R. Acad. Sci. II 321 (12) (1995) 501–506.
[16] T. Boutreux, P. de Gennes, Surface flows of granular mixtures: I. general principles and minimal model, J. Phys. I 6 (10) (1996) 1295–1304.
[17] T. Boutreux, E. Raphaël, P. de Gennes, Surface flows of granular materials: a modified picture for thick avalanches, Phys. Rev. E 58 (1998) 4692–4700.
[18] A. Aradian, É. Raphaël, P. de Gennes, Surface flows of granular materials: a short introduction to some recent models, C.R. Phys. 3 (2) (2002) 187–196.
[19] K. Hadeler, C. Kuttler, Dynamical models for granular matter, Granul Matter 2 (1) (1999) 9–18.
[20] K. Hadeler, C. Kuttler, Granular matter in a silo, Granul Matter 3 (2001) 193–197.
[21] C. Kuttler, On the competitive growth of two sand heaps, Math. Methods Appl. Sci. 26 (17) (2003) 1435–1449.
[22] K. Hadeler, D. Schieborn, Granular matter and the time-dependent viscous eikonal equation, Physica D 241 (5) (2012) 616–622.
[23] P. Cannarsa, P. Cardaliaguet, Representation of equilibrium solutions to the table problem of growing sandpiles, J. Eur. Math. Soc. 6 (2004) 1–30.
[24] P. Cannarsa, P. Cardaliaguet, G. Crasta, A boundary value problem for a PDE model in mass transfer theory: representation of solutions and applications, Calc. Var. 24 (4) (2005) 431–457.
[25] G. Crasta, S. Finzi Vita, An existence result for the sandpile problem on flat tables with walls, Netw. Heterog. Media 3 (2008) 815–830.
[26] P. Cannarsa, P. Cardaliaguet, C. Sinestrari, On a differential model for growing sandpiles with non-regular sources, Comm. Partial Diff. Eqs. 34 (7) (2009) 656–675.
[27] M. Falcone, S. Finzi Vita, A numerical study for growing sandpiles on flat tables with walls, in: IFIP Conference on System Modeling and Optimization, 202, 2005, pp. 127–137.
[28] M. Falcone, S. Finzi Vita, A finite-difference approximation of a two-layer system for growing sandpiles, SIAM J. Sci. Comput. 28 (2006) 1120–1132.
[29] M. Falcone, S. Finzi Vita, A Semi-Lagrangian scheme for the open table problem in granular matter theory, in: K. Kunisch, G. Of, O. Steinbach (Eds.), Numerical Mathematics and Advanced Applications, Springer, 2008, pp. 711–718.
[30] A. Lo Giudice, G. Giammanco, D. Fransos, L. Preziosi, Modelling sand slides by a mechanics-based degenerate parabolic equation, Math. Mech. Solids 24 (2019) 25582575.
[31] R.P. Chhabra, J.F. Richardson, Non-Newtonian Flow in the Process Industry: Fundamentals and Engineering Applications, Elsevier, 1999.
[32] C.W. Macosko, Rheology: Principles, Measurements and Applications, Wiley, 1994.
[33] R. Eymard, T. Gallouët, R. Herbin, Finite volume methods, in: Handbook of numerical analysis, 7, 2000, pp. 713–1018.
[34] R. Eymard, T. Gallouït, R. Herbin, A. Michel, Convergence of a finite volume scheme for nonlinear degenerate parabolic equations, Numer. Math. 92 (1) (2002) 41–82.
[35] M. Bessemoulin-Chatard, F. Filbet, A finite volume scheme for nonlinear degenerate parabolic equations, SIAM J. Sci. Comput. 34 (5) (2012) B559–B583.
[36] OpenFOAM: User Guide: Implementation details, 2020, [Online; accessed 16. Jul. 2020].
[37] N. Boulghobra, Climatic data and satellite imagery for assessing the aeolian sand deposit and barchan migration, as a major risk sources in the region of In-Salah (Central Algerian Sahara), Arab. J. Geosci. 9 (6) (2016) 450.
[38] Z.-C. Deng, L. Yang, An inverse problem of identifying the source coefficient in a degenerate heat equation, Inverse Probl. Sci. Eng. 23 (2015) 498–517.
[39] K. Beauchard, P. Cannarsa, M. Yamamoto, Inverse source problem and null controllability for multidimensional parabolic operators of grushin type, Inverse Probl. 30 (2014) 025006.
[40] P. Cannarsa, J. Tort, M. Yamamoto, Determination of source terms in a degenerate parabolic equatio, Inverse Probl 26 (2010) 105003.
[41] P. Cannarsa, P. Martinez, J. Vancostenoble, Global Carleman Estimates for Degenerate Parabolic Operators with Applications, Memoires of the American Mathematical Society, 2016.
[42] L. Yang, T. Lui, Z.-C. Deng, Multi-parameters identification problem for a degenerate parabolic equation, J. Comput. Appl. Math. 366 (2020) 112422.
[43] J. Tort, J. Vancostenoble, Determination of the insolation function in the nonlinear sellers climate model, Ann. I. H. Poincare-AN 29 (2012) 683–713.
[44] G. Fragnelli, G. Marinoschi, R.M. Mininni, S. Romanelli, Identification of a diffusion coefficient in strongly degenerate parabolic equations with interior degeneracy, J. Evol. Equ. 15 (2015) 27–51.
[45] M. Sepulveda, F. James, A. Coronel, Numerical identification of parameters for a model of sedimentation processes, Inverse Probl. 19 (2003) 951–972.
[46] Y.H. Ou, A. Hasanov, Z.H. Liu, Inverse coefficient problems for nonlinear parabolic differential equations, Acta Math. Sin. 24(10) 1617–1624.